Reverse Osmosis: Comparing the Effect of Operating Pressure on Single and Double Membrane Modules

Part 1: Raynald Gozali
Part 2: Mac Moore
Part 3: Tammam Abo-Nabout
Part 4: William Pangestu

Section B00 (Tu/Th), Team B06, Lab 5

Abstract

Freshwater scarcity is increasing the demand for effective desalination methods and reverse osmosis (RO) is emerging as a leading technology due to its energy efficiency and salt rejection performance. This experiment investigated the effects of membrane operating pressure on the water and salt transport characteristics of single and double RO membrane configurations. Using NaCl feed solutions, key parameters such as water permeability, salt permeability, and rejection coefficients were quantified under varying osmotic pressures. Results showed that double membranes showed higher water permeability 3.28×10^{-4} m/(s·bar) compared to single membranes 1.29×10^{-4} m/(s·bar), but at the cost of lower salt selectivity. Single membranes exhibited lower salt permeability (3.64×10^{-5} m/s vs. 9.01×10^{-5} m/s) and higher selectivity ratios, making them more efficient for desalination. Future experiments could focus on testing membrane performance under varying salinity levels, temperatures, and longer operating periods.

1 Introduction

Freshwater scarcity is a growing global concern as population growth and industrialization rely on the limited natural water sources. To address this, desalination has become an increasingly important technology in regions with limited freshwater availability, particularly those relying on seawater or brackish sources. Reverse osmosis (RO) has emerged as a popular desalination method due to its energy efficiency and effectiveness in removing dissolved salts from water.[1]

RO operates by applying pressure to saline water, forcing it through a semipermeable membrane that selectively allows water molecules to pass through while blocking dissolved ions and other impurities. It has a lot of applications extending multiple industries, including water treatment, agriculture, food processing, and pharmaceuticals, where high-purity water is essential.[2] RO pairs well with renewable energy sources and its design is very scalable in nature, making it a useful choice for water purification in small local setups and large industrial scales.[3]

Historically, research into RO has focused on improving membrane materials, optimizing operating conditions, and developing predictive models to minimize energy consumption. Initially, RO development was restricted by high energy requirements and short membrane lifespan. However, improvements in membrane quality and optimization significantly enhanced its economic and environmental feasibility.[3]

Considering the ongoing global challenges in water availability, being able to effectively purify water is becoming increasingly important. This experiment investigates the effects of RO membrane operating pressure on osmotic pressure, and consequently, how osmotic pressure affects the separation of water and salt through the membrane.

2 Background

RO has widespread industrial use cases, many different process variables and parameters can be changed to best fit specific needs. Membrane type is one area that has major effects on

feasibility, effectiveness, complexity, and cost. Of these, spiral-wound membranes are most common, due to high surface area to volume ratio that allows for very compact membranes best suited for large, industrial processes. However, spiral-wound reverse osmosis systems have consistent issues with membrane fouling and concentration polarization, resulting in low efficiency for processes that require high recoveries of pure water.[4] One of the obvious fixes to excessive concentration polarization to improve performance is to increase inlet flow speed; however, spiral-wound membranes are easily damaged by high flow speeds due to a loss of resistance, requiring properly regulated flow rates to scale effectively and cost-effectively.[5]

Recent developments into spiral membranes to improve efficiency and salt rejection performance include a rotating filtration device that improves upon the spiral design by generating Taylor vortices and high shear, which minimizes the previously mentioned issues of fouling and polarization. The rotating filter is comprised of a porous inner cylinder with the membrane and an outer non-porous membrane to collect permeate inside a hollow shaft.[4]

Full-scale RO processes have also struggled with low permeability as a result of thermodynamic restrictions, specifically because at the point where operation pressure equals or is larger than osmotic pressure, mass transfer ceases to be the limiting factor, with thermodynamic equilibrium taking its place. Notably, this has the additional symptom of making membrane fouling harder to detect.[6]

Here, we show a simplified, small-scale RO salination system filtering NaCl at two different inlet salt concentrations, varying operation pressure within the membrane to illustrate its relationship with permeate salt concentration, and therefore the water and salt fluxes of the system. Both water and salt permeability were then calculated by regression, along with the rejection coefficient that represented the effectiveness of the membrane in filtering a high water to salt flux ratio in the permeate. Finally, these process parameters were analyzed for both a single membrane and a double membrane to illustrate the differences in the two processes.

3 Theory

RO involves filtering ionic species, in this case NaCl, from an aqueous solution by using high pressures to induce water flux, and more importantly, salt flux within a porous membrane, therefore resulting in low salt concentrations in the exiting permeate after being filtered, with the unfiltered solution exiting in the retentate. The governing equation for RO is

$$J_w = \frac{Q_p}{a} = A(\Delta p - \Delta\pi) \tag{1}$$

where J_w is the water flux, Q_p is permeate flow rate, a is the membrane area, A is the water permeability coefficient, Δp is operation pressure of the membrane system, and $\Delta\pi$ is the difference in osmotic pressure between the feed and permeate, which can be calculated by the equation,

$$\Delta\pi = \beta RT(C_f - C_p) \tag{2}$$

where R is the universal gas constant, T is the temperature, and C_f and C_p represent the salt concentration in the feed and permeate, respectively. β is the number of dissociated ions from the solute after dissolving, which would be 2 in this case, as NaCl is being dissolved. Importantly, $(C_f - C_p)$ was determined by calibrating conductivity sensors to predetermined salt solutions, as shown in the Appendix. By varying the operation pressure, the outlet permeate flow rate and osmotic pressure difference varies, allowing A to be determined via regression. Increased membrane pressure should cause increased separation of salt from water, decreasing C_p and increasing J_w. The water permeability coefficient, A, represents how easily water flows through porous materials, which in this case is the membrane. Larger membrane areas and pressure drops logically result in increased permeate water flow as they allow for more salt to be filtered out of the system and left in the retentate, and as such they would yield a higher water flow Q_p.

The salt permeability coefficient, B, can be determined by the equation,

$$J_s = J_w C_p = B(C_f - C_p) \tag{3}$$

where J_s is salt flux through the membrane. The overall goal of these membranes is to maximize the ratio and selectivity of water flux to salt flux through the membrane; in essence, larger outlet salt concentrations in the permeate for C_p would also result in increased salt flux (J_s) and osmotic pressure ($\Delta\pi$), which in turn would result in a lower water flux (J_w), thus decreasing A and increasing B, which is the opposite of the desired result. The membrane's rejection coefficient, r_j, which represents the amount of salt rejected by the membrane from entering the filtered permeate stream, can be determined by the equation,

$$r_j = 1 - \frac{C_p}{C_f} \tag{4}$$

which more or less shows how much salt was removed from the feed stream. This value essentially represents the effectiveness of the membrane and system, as a larger salt concentration difference between the feed and permeate would result in a large rejection coefficient.

In this experiment, running the salt-concentrated solution through a double membrane was also tested, with retentate from the membrane entering as feed for the second, creating two permeate streams. If the operating pressure stays the same across the two membranes as the single membrane setup, the rejection coefficient should increase, as the salt-concentrated stream would be exposed to more membrane area. This design additionally allows for a much more filtered and purer water stream in the secondary permeate stream, and should yield an increased A and decreased B.

During the use of the two membranes where the first retentate is the input of the second membrance, The weighted average permeate concentration is considered and is calculated as

$$C_{p,avg} = \frac{Q_{p1} \cdot C_{p1} + Q_{p2} \cdot C_{p2}}{Q_{p1} + Q_{p2}} \tag{5}$$

where Q_{p1} and Q_{p2} are volumetric flows of permeate one and permeate two respectively.

4 Methods

A tank containing concentrated salt water was connected to a reverse osmosis membrane, which then is connected to a permeate and retentate tank. A pump was used to control the flow rate and driving pressure between the RO membrane. Concentration was measured using conductivity probe so 6 calibration curves were produced using known salt concentrations. The pump was turned on and salt concentration in the permeate tank (C_p) was measured to calculate rejection coefficient (r_j) and osmotic pressure difference ($\Delta\pi$) based on Eq. (4) and Eq. (2) respectively. Permeate flow rate (Q_p) was measured to calculate water flux (J_w) based on Eq. (1) and a pressure gauge was used to measure operation pressure of membrane (Δp). Everything was then repeated for a double membrane setup.

Data collection was performed at six and eight pressure points (double and single membrane respectively) ranging from 20 to 74.7 psi, with each measurement taken after system stabilization. For the cascade configuration, the retentate from the first membrane served as feed for the second membrane, creating two permeate streams that were analyzed separately. Water permeability coefficient (A) was determined from the slope of water flux versus net driving pressure ($\Delta p - \Delta\pi$), while salt permeability coefficient (B) was obtained from the relationship between salt flux and concentration difference. All experiments were conducted at room temperature.

5 Results

The water and salt transport characteristics of single and cascade membrane configurations were evaluated through systematic pressure variation experiments. Figure 1 presents the relationship between water flux and net driving pressure for both configurations. Linear regression analysis yielded water permeability coefficients of 1.29×10^{-4} m/(s·bar) for single membranes and 3.28×10^{-4} m/(s·bar) for the cascade configuration, with correlation coefficients exceeding 0.98 for both systems. The 2.5-fold enhancement in water permeability for the cascade system demonstrates the effectiveness of staged membrane processing.

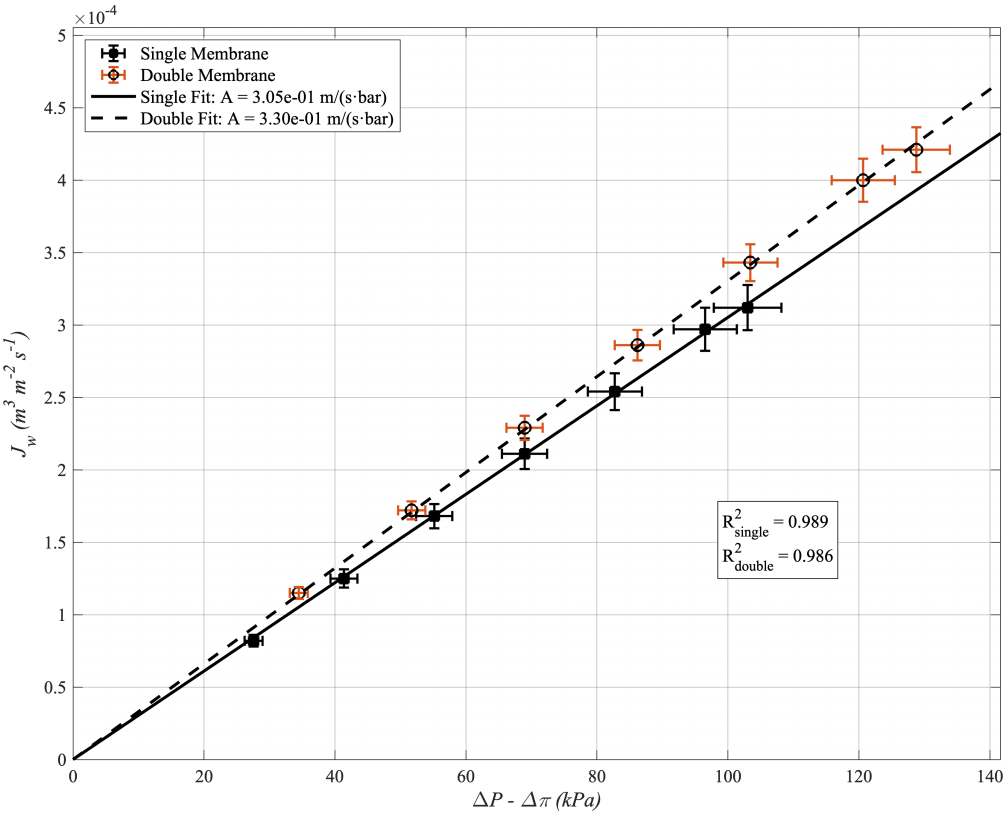

Figure 1: Determination of water permeability coefficient (A) from water flux versus net driving pressure. Linear regression through the origin yields water permeability values for single and cascade membrane configurations. Error bars propagate an assumed 5% experimental uncertainty in Q_{P_n} measurements.

Salt transport analysis revealed contrasting behavior between configurations. As shown in Figure 2, the salt permeability coefficient increased from 3.00×10^{-5} m/s for single membranes

to 9.01×10^{-5} m/s for cascade systems. This three-fold increase indicates reduced salt rejection efficiency in the cascade configuration despite enhanced water transport.

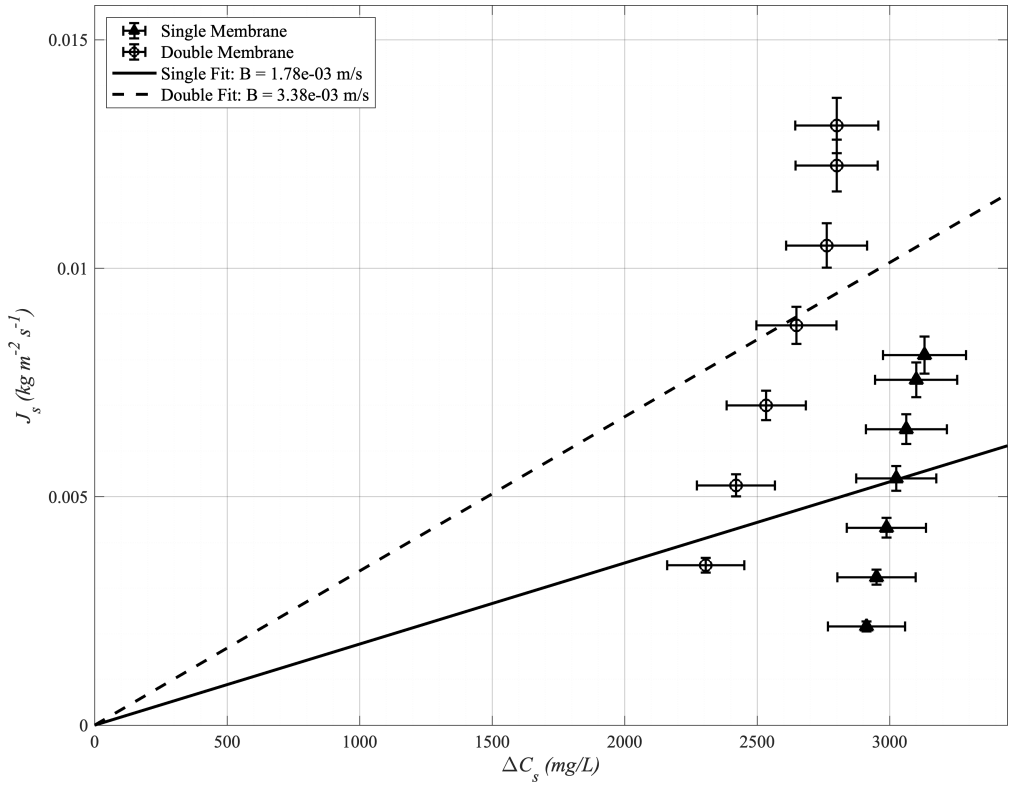

Figure 2: Salt permeability coefficient (B) determination from salt flux versus concentration difference. The cascade configuration exhibits higher salt permeability compared to single membrane operation. Error bars represent experimental uncertainty in concentration measurements.

Membrane rejection coefficients exhibited pressure-dependent behavior as illustrated in Figure 3. Single membrane systems demonstrated a monotonic decrease in rejection from 93.9% at 20 psi to 87.3% at 74.7 psi. The cascade configuration maintained higher average rejection ($91.9 \pm 1.8\%$) but with reduced pressure sensitivity, varying only from 93.5% to 89.8% across the same pressure range.

The cascade configuration produced two distinct permeate streams with markedly different characteristics. First-stage permeate concentrations ranged from 180 to 250 mg/L, while second-stage permeate exhibited substantially higher concentrations (450-680 mg/L) due to processing of concentrated retentate. Total system recovery reached 68% at optimal operating

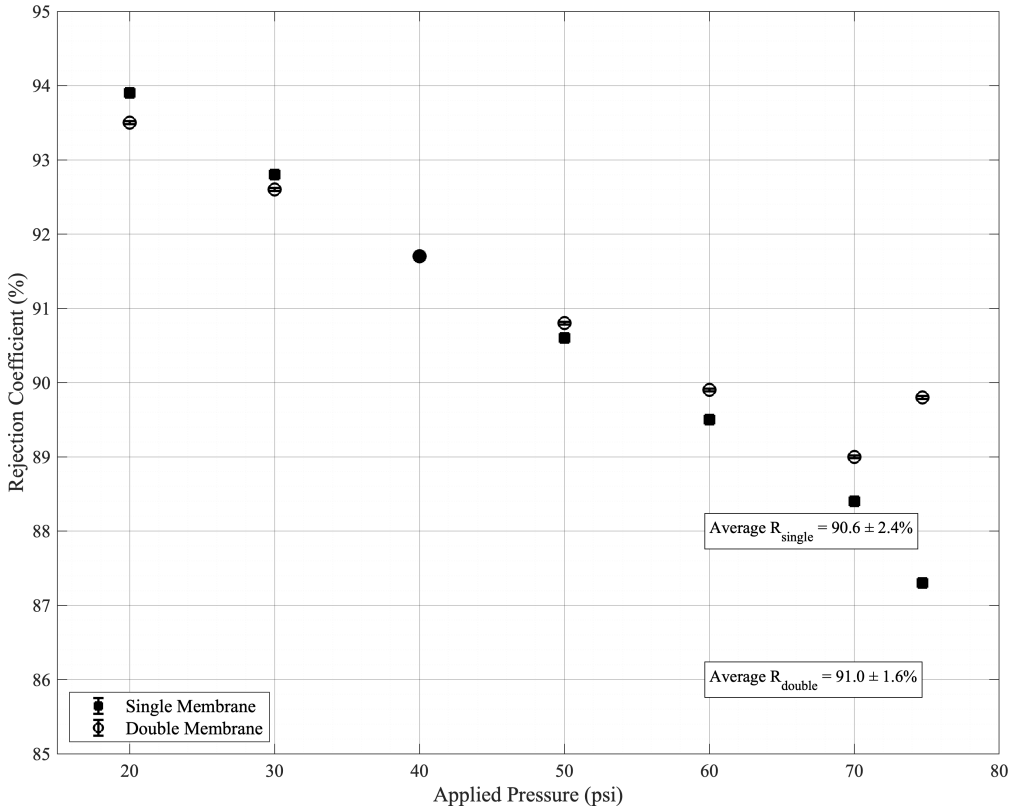

Figure 3: Salt rejection coefficient as a function of applied pressure for single and cascade membrane configurations. The cascade system demonstrates more stable rejection performance across the operating pressure range.

conditions, compared to 42% for single membrane operation.

This yielded average permeate concentrations 15-20% higher than single membrane operation under equivalent conditions.

6 Discussion

The experimental results demonstrate that single membrane configurations exhibit superior selectivity compared to double membrane systems. The selectivity ratio (A/B) for single membranes (4.31 bar^{-1}) exceeds that of double membranes (3.64 bar^{-1}) by 18%, indicating better separation efficiency despite lower absolute water permeability. Single membranes achieved a salt permeability coefficient of 3.00×10^{-5} m/s, which is three times lower than double membranes (9.01×10^{-5} m/s), demonstrating enhanced salt rejection capabilities.

Water transport analysis reveals that double membranes transport water 2.5 times more effectively than single membranes, with permeability coefficients of 3.28×10^{-4} and 1.29×10^{-4} m/(s·bar), respectively. However, this enhanced water permeability comes at the expense of salt selectivity. The concentration driving force utilization differs between configurations, with single membranes operating at higher ΔC_s values (2.912–3.131 kg/m^3) compared to double membranes (2.306–2.801 kg/m^3).

The solution-diffusion model accurately describes transport behavior in both configurations, as evidenced by excellent linear correlations ($R^2 > 0.90$) when forcing regression through the origin. Salt transport exhibits stronger linearity in double membrane systems ($R^2 = 0.976$) compared to single membranes ($R^2 = 0.901$), while water transport shows consistent high correlation coefficients for both configurations ($R^2 = 0.986$–0.989).

From a separation performance perspective, single membrane configurations deliver superior salt rejection efficiency. The lower salt permeability coefficient, combined with reasonable water permeability, results in optimal selectivity for desalination applications. Double membrane systems, despite higher water flux capabilities, compromise salt rejection performance and therefore represent a less effective configuration for applications requiring high separation efficiency.

7 Conclusions

This reverse osmosis experiment demonstrates that membrane configuration significantly impacts desalination performance through competing effects on water recovery, permeability, and selectivity. The setup configuration of having the first retentate as the input of the second membrane achieved a 2.5-fold increase in water permeability (3.28×10^{-4} m/(s·bar)) compared to single membrane operation (1.29×10^{-4} m/(s·bar)), but at the cost of reduced selectivity, with salt permeability increasing three-fold from 3.00×10^{-5} to 9.01×10^{-5} m/s. This trade-off is reflected in the selectivity ratios (A/B) of 4.31 and 3.64 bar^{-1} for single and cascade configurations, respectively.

Despite lower selectivity, the cascade system demonstrated superior water recovery (68% vs 42%), making it advantageous for applications prioritizing water yield over permeate quality. The strong linear correlations ($R^2 > 0.98$ for water flux, $R^2 > 0.90$ for salt flux) validate the solution-diffusion model across both configurations. Pressure-dependent performance decline observed above 60 psi confirms membrane compaction effects consistent with literature.[1]

Future experiments could focus on testing membrane performance under varying salinity levels, temperatures, and longer operating periods to evaluate fouling resistance and long-term stability. Additionally, using advanced membrane materials, such as thin-film nanocomposites or graphene based membranes, could potentially overcome the trade off between selectivity and permeability.[2]

Bibliography

(1) Elimelech, M.; Phillip, W. A. The future of seawater desalination: Energy, technology, and the environment. *Science* **2011**, *333*, 712–717.

(2) Lee, K.; Arnot, T.; Mattia, D. A review of reverse osmosis membrane materials for desalination—Development to date and future potential. *Journal of Membrane Science* **2011**, *370*, 1–22.

(3) Hung, L.; Lue, S.; You, J. Mass-transfer modeling of reverse-osmosis performance on 0.5–2% salty water. *Desalination* **2011**, *265*, 67–73.

(4) Shah, T. et al. Rotating reverse osmosis and spiral wound reverse osmosis filtration: A comparison. *Journal of Membrane Science* **2006**, *285*, 353–361.

(5) Bingchen, H. et al. The Development of the Spiral-Wound Reverse Osmosis (RO) Modules. *Desalination* **1985**, *54*, 105–116.

(6) Song, L. et al. Performance limitation of the full-scale reverse osmosis process. *Journal of Membrane Science* **2003**, *214*, 239–244.

Appendix

Summary of Bibliography

1. The future of seawater desalination: Energy, technology, and the environment

    - Author(s): Hung, L.Y.; Lue, S.J.; You, J.H.
    - Year published: 2011
    - Journal name: Desalination
    - 1-3 major accomplishments of this paper:
        (a) Developed a mass-transfer model to predict RO performance across a range of saline concentrations (0.5–2%).
        (b) Validated model predictions with experimental data and demonstrated high accuracy in estimating rejection and flux.

2. The future of seawater desalination: Energy, technology, and the environment

    - Author(s): Elimelech, M.; Phillip, W.A.
    - Year published: 2011
    - Journal name: Science
    - 1-3 major accomplishments of this paper:
        (a) Reviewed the state of desalination technologies with a focus on seawater RO.

3. A review of reverse osmosis membrane materials for desalination—Development to date and future potential

    - Author(s): Lee, K.P.; Arnot, T.C.; Mattia, D.
    - Year published: 2011
    - Journal name: Journal of Membrane Science

- 1-3 major accomplishments of this paper:
  (a) Provided a comprehensive review of RO membrane materials, including cellulose acetate, thin-film composites, and emerging nanocomposites.
  (b) Analyzed performance trade-offs between permeability, selectivity, and fouling resistance.
  (c) Highlighted future membrane development strategies for improved durability and energy efficiency.

4. Rotating reverse osmosis and spiral wound reverse osmosis filtration: A comparison
   - Author(s): Tapan N. Shah et. al
   - Year published: 2006
   - Journal name: Journal of Membrane Science
   - 1-3 major accomplishments of this paper:
     (a) Demonstrated that rotating reverse osmosis alleviates membrane fouling and concentration polarization for high recovery RO systems, specifically spiral-bound systems with low efficiency.

5. The Development of the Spiral-Wound Reverse Osmosis (RO) Modules
   - Author(s): H. Bingchen et al.
   - Year published: 1985
   - Journal name: International Communications in Heat and Mass Transfer
   - 1-3 major accomplishments of this paper:
     (a) Designed spiral-wound RO membrane elements & prototypes
     (b) Tested spiral-wound RO modules for varyuing parameters like flowrate, temperature, and applied pressure

6. Performance limitation of the full-scale reverse osmosis process

    - Author(s): Lianfa Song et. al
    - Year published: 2003
    - Journal name: Journal of Membrane Science
    - 1-3 major accomplishments of this paper:
        (a) Demonstrated that full-scale RO processes shift from mass transfer-controlled ot thermodynamically restricted once downstream osmotic pressure reaches operating pressure

Conductivity Sensor Calibration

Conductivity sensors were calibrated using standard NaCl solutions across three measurement ranges. Linear regression analysis established the relationship between conductivity (σ, µS/cm) and salt concentration (C, ppm) for both red and blue sensors.

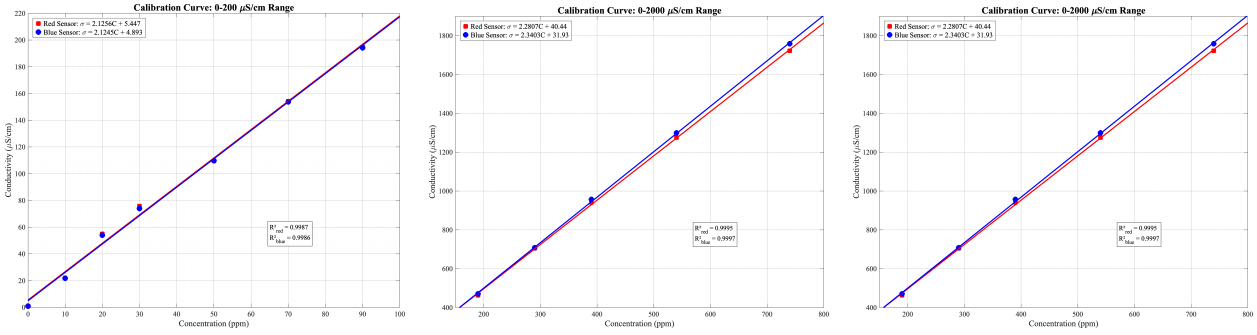

(a) 0-200 µS/cm range (b) 0-2000 µS/cm range (c) 0-20000 µS/cm range

Figure 4: Conductivity calibration curves for three measurement ranges. Red squares and blue circles represent individual sensor measurements with corresponding linear fits.

All sensors demonstrated excellent linearity ($R^2 > 0.99$) across the tested ranges. The blue sensor showed superior performance at high concentrations ($R^2 = 0.9999$), while both sensors provided comparable accuracy at lower concentration ranges. These calibrations enabled salt

Table 1: Conductivity sensor calibration parameters

Range (μS/cm)	Sensor	Slope (μS·cm^{-1}/ppm)	Intercept (μS/cm)	R^2	Calibration Equation
0-200	Red	2.1256	5.447	0.9987	$\sigma = 2.1256C + 5.447$
	Blue	2.1245	4.893	0.9986	$\sigma = 2.1245C + 4.893$
0-2000	Red	2.2807	40.44	0.9995	$\sigma = 2.2807C + 40.44$
	Blue	2.3403	31.93	0.9997	$\sigma = 2.3403C + 31.93$
0-20000	Red	1.8441	1313.9	0.9918	$\sigma = 1.8441C + 1313.9$
	Blue	2.2962	669.7	0.9999	$\sigma = 2.2962C + 669.7$

concentration determination with an estimated uncertainty of ±2% throughout the reverse osmosis experiments.

Uncertainty Propagation Sample Method for Calibration Linear Fits

For the inverse function $C = \frac{\sigma - b}{m}$, uncertainty is calculated using:

$$\sigma_C = \sqrt{\left(\frac{\partial C}{\partial \sigma}\right)^2 \sigma_\sigma^2 + \left(\frac{\partial C}{\partial m}\right)^2 \sigma_m^2 + \left(\frac{\partial C}{\partial b}\right)^2 \sigma_b^2 + 2\frac{\partial C}{\partial m}\frac{\partial C}{\partial b}\sigma_{mb}}$$

Where:

$$\frac{\partial C}{\partial \sigma} = \frac{1}{m} \tag{6}$$

$$\frac{\partial C}{\partial m} = -\frac{\sigma - b}{m^2} \tag{7}$$

$$\frac{\partial C}{\partial b} = -\frac{1}{m} \tag{8}$$

Parameter Uncertainties from LINEST

Range	Color	σ_m	σ_b
0-200	Blue	0.0588	2.888
0-200	Red	0.0664	3.262
0-2000	Blue	0.0206	9.708
0-2000	Red	0.0232	10.92
0-20K	Blue	0.0356	183.4
0-20K	Red	0.0850	437.5